Author Manuscript
Accepted for publication in a peer-reviewed journal

NIST National Institute of Standards and Technology • U.S. Department of Commerce

Published in final edited form as:
Appl Phys Lett. 2016 October 15; 109(15): . doi:10.1063/1.4963130.

Synchronization of Clocks Through 12 km of Strongly Turbulent Air Over a City

Laura C. Sinclair[1], **William C. Swann**[1], **Hugo Bergeron**[1,2], **Esther Baumann**[1], **Michael Cermak**[1], **Ian Coddington**[1], **Jean-Daniel Deschênes**[2], **Fabrizio R. Giorgetta**[1], **Juan C. Juarez**[3], **Isaac Khader**[1], **Keith G. Petrillo**[3], **Katherine T. Souza**[3], **Michael L. Dennis**[3], and **Nathan R. Newbury**[1]

[1]National Institute of Standards and Technology, 325 Broadway, Boulder, CO 80305, USA

[2]Université Laval, 2325 Rue de l'Université, Québec, Québec, G1V 0A6, Canada

[3]Johns Hopkins Applied Physics Laboratory, 11100 Johns Hopkins Rd, Laurel, MD 20723, USA

Abstract

We demonstrate real-time, femtosecond-level clock synchronization across a low-lying, strongly turbulent, 12-km horizontal air path by optical two-way time transfer. For this long horizontal free-space path, the integrated turbulence extends well into the strong turbulence regime corresponding to multiple scattering with a Rytov variance up to 7 and with the number of signal interruptions exceeding 100 per second. Nevertheless, optical two-way time transfer is used to synchronize a remote clock to a master clock with femtosecond-level agreement and with a relative time deviation dropping as low as a few hundred attoseconds. Synchronization is shown for a remote clock based on either an optical or microwave oscillator and using either tip-tilt or adaptive-optics free-space optical terminals. The performance is unaltered from optical two-way time transfer in weak turbulence across short links. These results confirm that the two-way reciprocity of the free-space time-of-flight is maintained both under strong turbulence and with the use of adaptive optics. The demonstrated robustness of optical two-way time transfer against strong turbulence and its compatibility with adaptive optics is encouraging for future femtosecond clock synchronization over very long distance ground-to-air free-space paths.

Future precise optical clock networks will enable a wide range of applications including precision navigation and timing, coherent phased-arrays, tests of geodesy, time distribution based on an optical standard, searches for dark matter or gravity waves, and many others [1–10]. As a step towards such networks, we recently demonstrated an optical two-way time-frequency transfer (O-TWTFT) technique that can support femtosecond-level phase (time) comparison [11] and real-time femtosecond-level synchronization [12,13] of two clocks across a free-space optical link. These demonstrations, however, were conducted at moderate atmospheric turbulence strengths over 2 to 4 km air paths. Ultimately, systems will need to operate over longer paths with stronger integrated turbulence.

SUPPLEMENTARY MATERIAL
Supplementary Figure 1 gives the details on the design of the tip/tilt FSO terminal. Supplementary Figure 2 gives histograms of the detected comb power and link availability. Supplementary Figure 3 gives high time resolution examples of time excursions during a signal dropout.

Turbulence presents two significant challenges. First, the zeroth-order 'piston mode' leads to fluctuations in the one-way optical time-of-flight between clocks. In O-TWTFT, this effect is removed through a two-way comparison of the clock time offsets, relying on the fundamental reciprocity of bi-directional single spatial mode propagation [14,15]. Here, we demonstrate this time-of-flight reciprocity supports sub-femtosecond synchronization not only in weak integrated turbulence, corresponding to single scattering of the transmitted light, but also in strong integrated turbulence, corresponding to multiple scattering. Second, turbulence causes scintillation, beam distortion and beam pointing variations that all lead to fluctuations of the received light intensity into the receiver's single mode optical fiber. Fluctuations extending below the detection threshold result in a signal "dropout" and no exchange of timing information. These dropouts increase significantly in stronger integrated turbulence, reaching rates of over 100 per second. In addition, dropouts due to beam obstruction and platform misalignment can occur. Here, we show that O-TWTFT is indeed robust enough overcome these effects from strong turbulence.

We implement O-TWTFT over a 12-km horizontal path that is close to the ground (25-50 m elevation) over an urban environment; it thus experiences much greater integrated turbulence than a ground-to-air path. The turbulence structure function reaches $C_n^2 \sim 10^{-13}\ m^{-2/3}$, corresponding to a Rytov variance of 7.5, which is well into the strong turbulence regime [16]. We demonstrate operation in four different configurations with: (i) a remote clock based on either an optical or microwave oscillator and (ii) free-space optical (FSO) terminals based on either tip-tilt correction or adaptive optics.

Figure 1a shows a top-level diagram of the O-TWTFT setup described in detail in Ref. [12,13]. Each clock output is the labeled pulse train output from a 200-MHz optical frequency comb phase-locked to a local oscillator. At the master site, the local oscillator is a cavity-stabilized laser. At the remote site, the local oscillator is either a second cavity-stabilized laser or a 10-GHz dielectric resonator oscillator disciplined to a quartz oscillator. This microwave oscillator has higher free-running timing noise than the optical oscillator, but is less expensive, more compact and rugged. The time at each site is defined by the arrival of the frequency comb pulses at a calibrated reference plane.

The two-way time transfer operates through the coherent exchange of frequency comb pulses between sites. The arrival time of the incoming pulses are measured with femtosecond precision through linear optical sampling, which requires a transfer frequency comb in addition to the clock comb at the master site [12]. In addition, a "coarse" TWTFT is implemented via a phase-modulated cw laser to remove timing ambiguities and provide additional required timing information. This same phase modulated cw laser transmits the measured timing data from the master to the remote site, where they are combined in a master synchronization equation (Eq. (1) of Ref. [12]) to calculate the clocks' time offset, ΔT_{calc}, at a chosen reference plane. ΔT_{calc} is input to an adaptive Kalman-filter-based loop filter whose output adjusts the remote clock time with an overall effective synchronization feedback bandwidth of ~10 to ~100 Hz for a remote optical or microwave oscillator, respectively. The folded path geometry (See Fig. 1.) enables an out-of-loop measurement over a short fiber link of the clocks' time offset, ΔT, through heterodyne detection between

the two clock combs' pulse trains at a common reference plane [12]. All data reported here use this out-of-loop measurement ΔT.

The master and remote transceivers, including the frequency combs, field-programmable gate array controllers, linear optical sampling detection, and phase-modulated cw light source [17], reside in one room while the FSO terminals are in an adjacent room with open windows to access the air path. The transceivers and terminals are connected via 20 meters of polarization-maintaining dispersion-shifted fiber to minimize stretching of the comb pulses. Three optical signals are transmitted: the frequency comb pulse trains, the phase-modulated cw laser, and a beacon cw laser for alignment of the terminals. The frequency comb outputs ~5 mW in the detection bandwidth. The phase-modulated cw light and beacons are ~5 mW and ~20 mW, respectively. The combined beam meets the American National Standards Institute (ANSI) standard for eye safety with aided viewing [18]. The terminals launch and receive these signals across the 11.6-km link that is folded by a flat mirror. (See Fig. 1b.) The pointing of this flat folding mirror is manually adjusted via a cellular data connection every few hours to maintain alignment over diurnal temperature cycles.

O-TWTFT puts significant requirements on the terminals as they must launch and receive from single-mode optical fiber, have low insertion loss, and be fully reciprocal (bi-directional) without spurious reflections. We operated with two different pairs of terminals. One pair of custom terminals were constructed with a low 1.5-dB insertion loss, tip/tilt correction of turbulence-induced beam wander, a 5-cm physical aperture diameter, and a 4-cm launched $1/e^2$ beam diameter, which approximately matches the Fried parameter for moderate turbulence over 12 km [16]. (See Supplementary Figure 1). We also operated with a pair of commercial FSO terminals that applied adaptive optics (AO) correction of the turbulence-induced beam distortions for the first thirty-five Zernike modes [19]. These terminals had a 5-dB insertion loss, 10-cm physical aperture diameter, and a 10-cm launched $1/e^2$ beam diameter [20]. The larger aperture of the AO over the tip/tilt terminals provides a gain of 12 dB. However, the net gain is reduced by the higher insertion loss and required power threshold, discussed below, both of which could be avoided in a custom AO terminal.

Table 1 summarizes five different data runs classified by the terminal (AO or tip/tilt) and underlying oscillator for the remote clock (optical or microwave). The measurements spanned six months and thus covered different weather and experienced turbulence strengths ranging from weak ($C_n^2 \sim 10^{-16}$) to moderate ($C_n^2 \sim 10^{-14}$-10^{-15}) to strong ($C_n^2 \sim 10^{-13}$-10^{-14}), with $C_n^2 \sim 10^{-13}$ corresponding to a Rytov variance of 7.5 over our 11.6-km link [16]. The detection threshold is ~2.5 nW for the tip/tilt terminals and ~ 13 nW for the AO terminals. (Spurious reflections within the AO terminals required a higher detection threshold.) Received power below these values results in a dropout. In this case the remote clock is "free-running" with timing corrections based on a Kalman filter [13]. (See Supplementary Fig. 2 for histograms of the received powers).

As with free-space optical communications [21], the duration of the signal dropouts is critical. Figure 2 gives the probability distribution, $P_d(\tau_d)$, in unit of s^{-2}, of a dropout of duration τ_d per second. (The average link availability in Table 1 is $L.A. = \int \tau_d P_d(\tau_d) d\tau_d$.)

The number of dropouts per second varies from 114 s^{-1} to 10 s^{-1} from strong to moderate turbulence for the tip-tilt terminals. However, the vast majority of dropouts have a duration below the time constant of the feedback loop (1.6 – 16 ms), and therefore have negligible effect. The much rarer long dropouts (> 1 sec) can lead to large remote clock time excursions, depending on the remote clock's oscillator stability.

We can disentangle these effects of signal dropouts from a more fundamental breakdown of O-TWTFT due to turbulence by separating the results into "continuous" data sampled even during dropouts and "gated" data that includes only periods of active synchronization (i.e. excludes signal dropouts and the subsequent resynchronization). This gating is based on available real-time signals including received power and ΔT_{calc}. Indeed, this division of continuous and gated operation carries over to system design considerations for future applications of clock networks.

Figure 3 shows the turbulence structure function, C_n^2, and synchronization performance as measured by ΔT for gated and continuous data for each data run. (The continuous data fall directly underneath the gated data and are often not visible). In general, long signal dropouts lead to large time excursions, which appear as vertical lines deviating far from zero for these 1-second averaged data. Over finer timescales, these time excursions appear as an increasing time offset followed by rapid resynchronization at the end of the dropout (see Ref. [13] and Supplementary Fig. 3).

Fig. 3a shows data for tip-tilt terminals with an optically based remote clock under both moderate and strong turbulence conditions (first two rows of Table 1). There is no observable difference in synchronization between moderate and strong turbulence. The two ~4-hr periods are a portion of a longer 11.5-hr data run (which had poor link availability in the middle due to misalignment of the folding mirror). Over the total 11.5 hours, one-way time-of-flight varied by ~200 ps primarily due to air temperature but the synchronized clocks agreed to 21 fs during active synchronization (i.e. gated data) and were within 370 fs over all time (continuous data) at 1-s averaging. Figure 3b shows similar ~ 4-hour data for a microwave-based remote clock (third row of Table 1) with 17 fs and 600 fs (off-scale) peak-to-peak time wander for gated and continuous data, respectively. This 600-fs time wander reflects the higher random walk of the microwave oscillator compared to the optical oscillator during long dropouts. Figure 3c–d show similar data for the AO terminals operating during a period of light haze (rows 3–4 of Table 1). The higher white noise is due to digitization issues in the out-of-loop measurement rather than real performance degradation. Large time excursions are observed in the continuous data, as expected from the long duration dropout tail in Fig. 2. However, large time excursions also appear in the gated data induced by spurious double reflections within the AO terminals, which trigger a false timing measurement. (These false timing measurements cause the apparent positive bias of the large time excursions of Fig. 3c–d for both the gated and continuous data.) These limitations are not fundamental and could be eliminated with improved terminal design.

Figure 4a shows the time deviation for the continuous data of Fig. 3. In all cases, the time deviation is flat or increasing out to ~3-4 s averaging time, corresponding to the presence of 100-ms to 10-s duration dropouts and the corresponding time excursions. Because of the

larger random walk of the microwave-based remote clock than an optically-based clock, the time deviation is ~3-10× higher. However, the time deviation is always below 10 fs beyond 100 s averaging. Fig 4b shows the time deviation for gated data for the tip-tilt terminals. For the AO terminals the time deviation for the gated data is similar to that of the continuous data because of the aforementioned time excursions due to spurious reflections. Again, there is no significant difference between moderate and strong turbulence. (The statistical uncertainty of each point is negligible, but the true uncertainty depends on the probability distribution of dropouts since the time deviation calculation performs an interpolation during the gated period.) Beyond 2-s averaging time, the time deviation is below 1 femtosecond and reaches 165 attoseconds at hundreds of seconds averaging time for an optically-based remote clock (even dropping below the data of Ref. [12] due to better laboratory temperature control).

Future applications of O-TWTFT will require spanning long distances, across terrestrial links or links to air-borne or even space-based platforms. With increased distance, especially for near-horizontal air paths, the effects of atmospheric turbulence become more important. Here, we have shown the synchronization of a remote clock to a master optical clock across a turbulent 12 km horizontal air path over an urban environment. The synchronization performance is at the same level as previous O-TWTFT over lower turbulence and shorter 2-4 km paths. These results are in good agreement with theoretical treatments that the atmospheric reciprocity should still support O-TWTFT even at 100 km ground-to-space paths [15]. Furthermore, O-TWTFT is compatible with adaptive optics FSO terminals, which may be needed for very long distance time transfer. Synchronization at these very strong integrated turbulence levels bodes well for the use of optical clock networks in tests of fundamental physics or the redefinition of the second.

Supplementary Material

Refer to Web version on PubMed Central for supplementary material.

Acknowledgments

We acknowledge funding from the Defense Advanced Research Projects Agency Defense Sciences Office PULSE program and helpful comments from Dave Howe, Kevin Cossel, and Marla Dowell. The views, opinions and/or findings expressed are those of the author and should not be interpreted as representing the official views or policies of the Department of Defense or the U.S. Government.

References

1. Riehle F. Towards a redefinition of the second based on optical atomic clocks. Comptes Rendus Phys. 2015; 16:506.
2. Delva P, Lodewyck J. Atomic clocks: new prospects in metrology and geodesy. Acta Futura. 2013; 7:67.
3. Chou CW, Hume DB, Rosenband T, Wineland DJ. Optical Clocks and Relativity. Science. 2010; 329:1630. [PubMed: 20929843]
4. Schiller S, Tino GM, Gill P, Salomon C, Sterr U, Peik E, Nevsky A, Görlitz A, Svehla D, Ferrari G, et al. Einstein Gravity Explorer-a medium-class fundamental physics mission. Exp Astron. 2009; 23:573.

5. Altschul B, Bailey QG, Blanchet L, Bongs K, Bouyer P, Cacciapuoti L, Capozziello S, Gaaloul N, Giulini D, Hartwig J, et al. Quantum tests of the Einstein Equivalence Principle with the STE–QUEST space mission. Adv Space Res. 2015; 55:501.
6. Wolf P, Blanchet L. Analysis of Sun/Moon gravitational redshift tests with the STE-QUEST space mission. Class Quantum Gravity. 2016; 33:35012.
7. Cliche J-F, Shillue B. Precision timing control for radioastronomy: maintaining femtosecond synchronization in the Atacama Large Millimeter Array. IEEE Control Syst. 2006; 26:19.
8. Derevianko A, Pospelov M. Hunting for topological dark matter with atomic clocks. Nat Phys. 2014; 10:933.
9. Van Tilburg K, Leefer N, Bougas L, Budker D. Search for Ultralight Scalar Dark Matter with Atomic Spectroscopy. Phys Rev Lett. 2015; 115:11802.
10. Loeb A, Maoz D. Using Atomic Clocks to Detect Gravitational Waves. ArXiv150100996 Astro-PhIM. 2015
11. Giorgetta FR, Swann WC, Sinclair LC, Baumann E, Coddington I, Newbury NR. Optical two-way time and frequency transfer over free space. Nat Photonics. 2013; 7:434.
12. Deschênes J-D, Sinclair LC, Giorgetta FR, Swann WC, Baumann E, Bergeron H, Cermak M, Coddington I, Newbury NR. Synchronization of Distant Optical Clocks at the Femtosecond Level. Phys Rev X. 2016; 6:021016.
13. Bergeron H, Sinclair LC, Swann WC, Nelson CW, Deschênes J-D, Baumann E, Giorgetta FR, Coddington I, Newbury NR. Tight real-time synchronization of a microwave clock to an optical clock across a turbulent air path. Optica. 2016; 3:441.
14. Shapiro JH. Reciprocity of the Turbulent Atmosphere. J Opt Soc Am. 1971; 61:492.
15. Robert C, Conan J-M, Wolf P. Impact of turbulence on high-precision ground-satellite frequency transfer with two-way coherent optical links. Phys Rev A. 2016; 93:33860.
16. Andrews, LC., Phillips, RL. Laser beam propagation through random media, Laser Beam Propagation through Random Media. 2nd. SPIE; Bellingham, WA: 2005.
17. Sinclair, LC., Swann, WC., Deschênes, J-D., Bergeron, H., Giorgetta, FR., Baumann, E., Cermak, M., Coddington, I., Newbury, NR. Slow Light Fast Light Opto-At Precis Metrol IX. SPIE; San Francisco, California, USA: 2016. Optical system design for femtosecond-level synchronization of clocks; p. 976308
18. ANSI Z136.6-2005. American National Standard for Safe Use of Lasers Outdoors. Laser Institute of America; 2005.
19. Noll RJ. Zernike Polynomials and Atmospheric Turbulence. J Opt Soc Am. 1976; 66:207.
20. Juarez, JC., Young, DW., Venkat, RA., Brown, DM., Brown, AM., Oberc, RL., Sluz, JE., Pike, HA., Stotts, LB. Analysis of link performance for the FOENEX laser communications system. In: Thomas, L., Spillar, E., editors. Atmospheric Propag IX. SPIE; 2012. p. 838007
21. Leclerc, TT., Phillips, RL., Andrews, LC., Crabbs, R. Buffer requirements of an optical communication system in atmospheric turbulence. Thomas, LM Wasiczko, Spillar, EJ., editors. 2013. p. 87320A

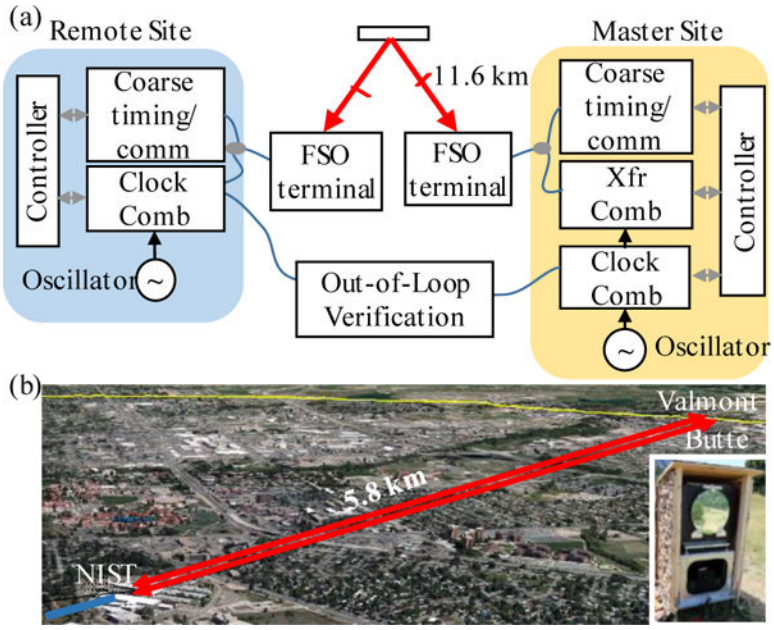

FIG. 1.

System Overview. (a) At each site, a clock is constructed from a frequency comb phase-locked to an optical or microwave oscillator. At the master site, a second transfer frequency comb is needed [12,13,17]. Each site's comb is wavelength multiplexed with a modulated cw laser for coarse TWTFT and data communication. The timing information is collected at the remote site, where the time offset is calculated and fed back to the remote clock to synchronize its time to the master clock. The folded path geometry (red lines) allows for a direct "out-of-loop" comparison of the clocks' time offset. FSO: free-space optical (b) Signals are launched from a terminal at NIST, reflected off a flat mirror 5.8 km away on Valmont Butte (right inset), finally returning to a second terminal in the same roof-top laboratory. The turbulence structure function is measured by a scintillometer over a 1 km adjacent path (blue line) or extracted from the received comb intensity fluctuations.

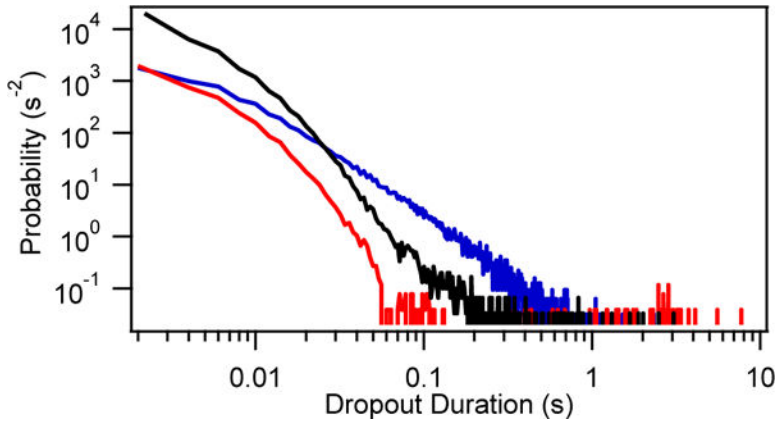

FIG. 2.

Probability distribution of dropout duration for the tip-tilt terminals under strong turbulence (black line) and moderate turbulence (red line), e.g. rows 1–2 of Table 1, and for the AO terminal (blue line) under weak-to-moderate turbulence but hazy conditions, e.g. row 4 of Table 1.

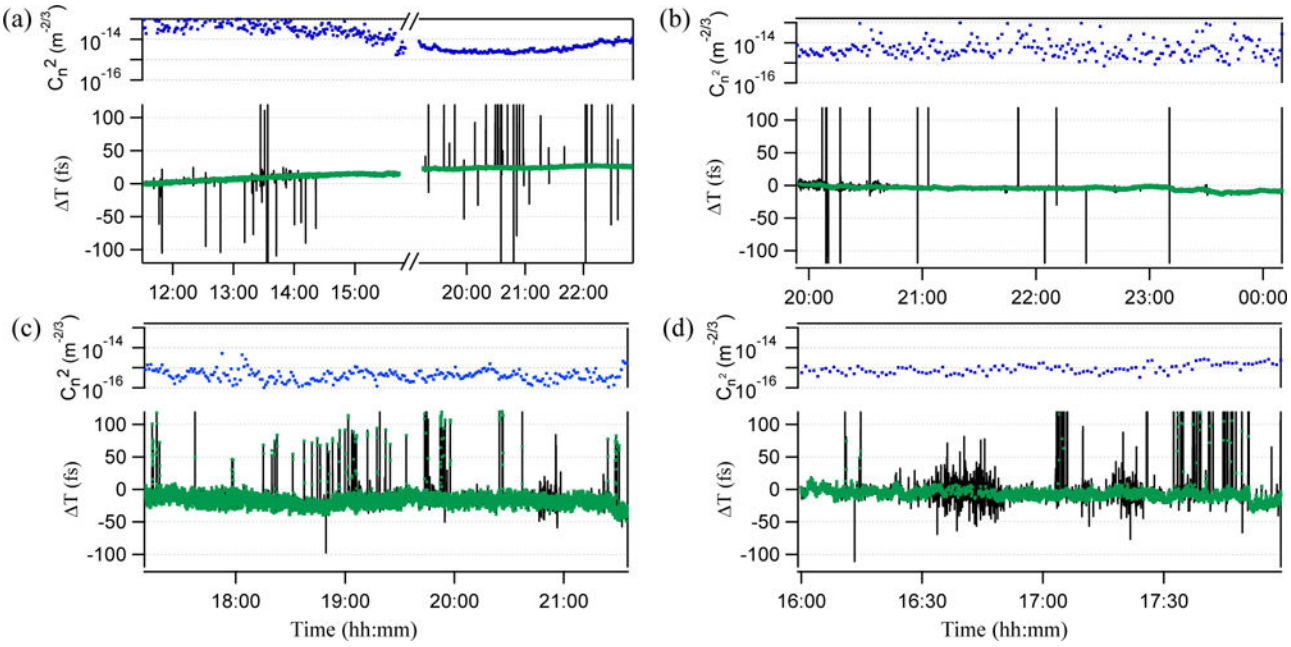

FIG. 3.

Synchronization of the clock times, ΔT, under continuous (black lines) and gated (green dots) operation and the turbulence structure function, C_n^2 (blue dots), for (a) tip/tilt terminals with an optically-based remote clock under strong (11:30 to 16:00) and moderate (19:00 to 23:00) turbulence, (b) tip/tilt terminals with a microwave-based remote clock, (c) AO terminals with an optically-based remote clock, and (d) AO terminals with a microwave-based remote clock. All data averaged at 1 second.

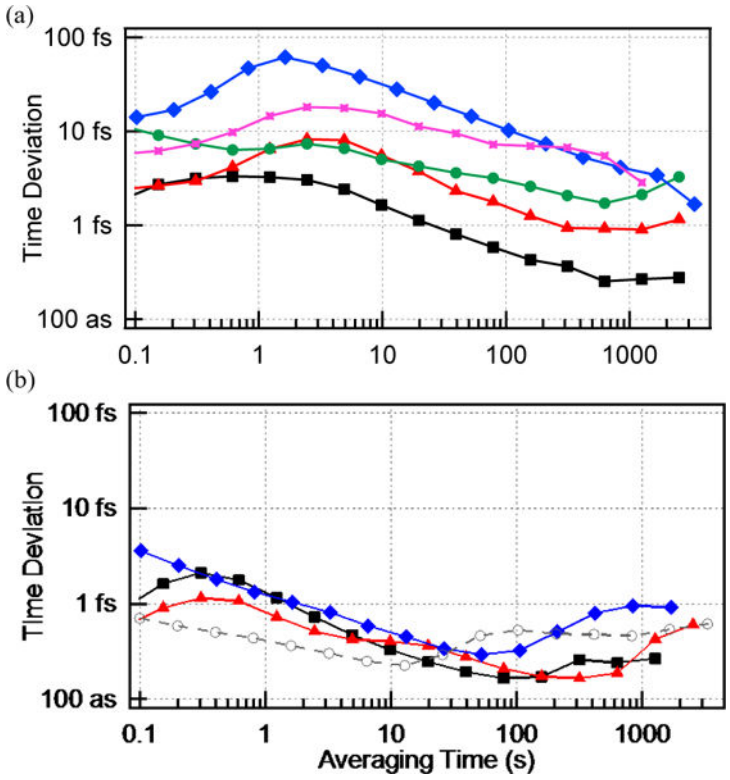

FIG. 4.

(a) Time deviation calculated from continuous data for tip-tilt terminals with an optically based remote clock over strong turbulence (black squares) and over moderate turbulence (red triangles), and with a microwave-based clock (blue diamonds), as well as for the AO terminals with an optically based remote clock (green circles) and microwave-based remote clock (pink stars). (b) Time deviation calculated from gated data for the tip-tilt terminals (same color coding as in part (a)). Time deviation from previous data over a 4-km link at lower turbulence is shown (grey open circles) [12].

TABLE I

Summary of measurements

Oscillator at Remote Clock Site	FSO terminal	C_n^2 ($m^{-2/3}$)	Average Link Availability (%)	Figure
Optical	Tip/Tilt	$10^{-14} - 10^{-13}$	68	3a
Optical	Tip/Tilt	$10^{-15} - 10^{-14}$	95	3a
Microwave	Tip/Tilt	$10^{-15} - 10^{-14}$	65	3b
Optical	AO	$10^{-16} - 10^{-15}$	86	3c
Microwave	AO	$\sim 10^{-15}$	86	3d